Available online at www.sciencedirect.com
ScienceDirect
Journal of Computational Physics 225 (2007) 1673–1694
JOURNAL OF COMPUTATIONAL PHYSICS
www.elsevier.com/locate/jcp

Condensed history Monte Carlo methods for photon transport problems

Katherine Bhan, Jerome Spanier *

Beckman Laser Institute and Medical Clinic, 1002 Health Science Road E., University of California, Irvine, CA 92612, United States

Received 24 May 2006; received in revised form 6 February 2007; accepted 7 February 2007
Available online 22 February 2007

Abstract

We study methods for accelerating Monte Carlo simulations that retain most of the accuracy of conventional Monte Carlo algorithms. These methods – called Condensed History (CH) methods – have been very successfully used to model the transport of ionizing radiation in turbid systems. Our primary objective is to determine whether or not such methods might apply equally well to the transport of photons in biological tissue. In an attempt to unify the derivations, we invoke results obtained first by Lewis, Goudsmit and Saunderson and later improved by Larsen and Tolar. We outline how two of the most promising of the CH models – one based on satisfying certain similarity relations and the second making use of a scattering phase function that permits only discrete directional changes – can be developed using these approaches. The main idea is to exploit the connection between the space-angle moments of the radiance and the angular moments of the scattering phase function. We compare the results obtained when the two CH models studied are used to simulate an idealized tissue transport problem. The numerical results support our findings based on the theoretical derivations and suggest that CH models should play a useful role in modeling light-tissue interactions.

Keywords: Monte Carlo methods; Condensed history models; Radiative transport equation

1. Introduction

The physics of light propagation in tissue dictates that a typical photon will interact with the scattering centers of the tissue thousands of times for each millimeter of travel and that the vast majority of these interactions will change the photon direction only slightly. More specifically, the photon mean free path (mfp) in tissue is typically 10–50 μm and the ratio of absorption to scattering is frequently much less than 0.01. Moreover, the average cosine, g, of the scattering angle (the angle between the unit vectors that describe the directions of travel before and after collision) in tissue is in the range 0.7–0.9 so that many individual collisions are required to deflect photons substantially from their initial orientations when directed into a tissue surface. These conditions, which are of interest when using laser probes to interrogate biological tissue, are similar

* Corresponding author. Tel.: +1 949 824 3419; fax: +1 949 824 6969.
E-mail addresses: kbhan@uci.edu (K. Bhan), jspanier@uci.edu (J. Spanier).

0021-9991/$ - see front matter © 2007 Elsevier Inc. All rights reserved.
doi:10.1016/j.jcp.2007.02.012

to those describing electron transport at high energies, for which typical electrons undergo $\sim 10^5$ collisions before slowing down. Under such conditions, the large computing costs associated with processing each photon or electron history in detail makes analog Monte Carlo (MC) simulations quite expensive. For such problems, it is therefore desirable to replace the exact probability model on which the conventional MC simulation is based by an approximate probability model in which a very large number of individual events are compressed into much fewer "super-events", so that simulations based on this approximate model are much faster, yet sufficiently accurate to support reliable predictions. In this paper we discuss how these ideas, developed originally for electrons and referred to as Condensed History (CH) models, might usefully be carried over to the MC simulation of photons.

In Sections 2–4 we provide an overview of some methods previously suggested for CH models and outline a theoretical context for understanding them. We then, in Sections 5 and 6, describe our recent work applying two of the most promising of these CH models to photon transport. We provide numerical evidence (Sections 7 and 8) that one of these – the discrete scattering angles (DSA) approach – produces advantages over a second one studied that is based on similarity theory (ST). In Section 9, we develop an analysis of the factors that lead to an understanding of the tradeoffs required to balance efficiency and accuracy for CH models. Finally, in Section 10, we summarize our results and present some ideas for future investigation stimulated by them. Appendices A and B present derivations used in this paper.

2. Overview

We describe in this section some ideas that have been successfully applied to electron transport for many years. We also mention one method, based on similarity theory, that appears to have been introduced with photon transport in mind.

The idea of replacing the detailed "collision-by-collision" MC model by a multiple collision model to speed up computations is due to Berger [1], and will be called here the Classical Condensed History (CCH) model. In simulations based on one of Berger's original formulations of this model, particles travel a *fixed*, user-defined, distance s between successive collisions, where s is deliberately chosen to be larger than the mean free path (mfp) in the medium. To accommodate this artificial selection of intercollision distances, the scattering angle is sampled from a probability density function (pdf) derived from the original single scattering pdf, f (sometimes called the differential scattering cross-section) that represents multiple scattering events. In the CCH model, the multiple scattering pdf is called the Goudsmit–Saunderson [2] (GS) probability density function, designated here by f_{GS}; it is the *exact*[1] conditional pdf for the multiple scattering angle, conditioned upon traveling a fixed, but arbitrary distance $s > 0$ between successive (multiple) collisions. While the CCH model has made it possible to apply Monte Carlo methods to electron transport in problems that would otherwise be prohibitively costly to simulate, it has several shortcomings. Apart from energy-dependent effects, such as the neglect of energy straggling in the approach based on the continuous slowing down approximation [3], these all stem in one way or another from the rigid way of sampling intercollision distances. As a result, various attempts to improve upon the CCH method have been attempted [4,5].

The approach that is adopted here can be traced to work of Lewis [6], Goudsmit and Saunderson [2], and Larsen and Tolar [7,8]. We refer to this general philosophy as the Lewis–Larsen theory. This approach is based on the observation that accuracy in a CH model might be based upon the replacement of the single scattering pdf by another that preserves a certain number of low-order angular moments of the original. The so-called similarity theory (ST) suggested by Wyman et al. [9] represents one attempt to use this approach to accelerate the simulation of photons, while the more recent suggestion by Prinja and Franke [10] to replace the original scattering pdf by one based exclusively on a discrete set of scattering angles (DSA), is another that was proposed for electron transport. For both of these methods the Lewis–Larsen theory provides a theoretical context.

In the next section, we review briefly the CH models that were stimulated by Berger's seminal paper in our attempt to explore their advantages and shortcomings for photon transport. In the section that follows, we

[1] The GS probability density function is exact provided that energy losses along the path are disregarded. Since our primary interest in this paper is in light transport, for which it is usual to assume a constant velocity, we make this assumption here and throughout the paper.

outline the Lewis–Larsen theory that helps to frame our understanding of how to achieve a proper combination of both speed and accuracy in a CH simulation and discuss briefly Larsen and Tolar's attempts to restore the fully stochastic nature of CH modeling within this framework. The next two sections present our ideas for the approaches based on ST theory and on the use of DSA.

3. The CCH and related models

The CCH model and its variants have been applied with success to electron transport in large tissue systems (e.g. simulating the full body radiation dose delivered in treating cancer by ionizing radiation) [11,12]. However, it is clear that CCH modeling cannot be very useful in tissue samples whose optical dimensions are comparable to the particle mean free path. In such problems, radiation could easily penetrate the tissue without, or with minimal, angular deflection making simulation relatively insensitive to the scattering properties of the tissue. In fact, for optically thin samples any approximate Monte Carlo method is likely to be less efficient than analog Monte Carlo. Of course, it must be borne in mind that CCH simulation with a fixed step size produces a radiation field that fails to satisfy the radiative transport equation (RTE), so it must be regarded as an approximate transport model. In this respect, it competes with all other approximate RTE solvers, including deterministic ones based on various numerical approximations to the RTE.

Considerable effort has been expended to modify the CCH algorithm to mitigate the effect of fixing inter-collision distances and improve the space-angle distribution of radiation. One idea is to split the total distance s to be traveled in each step into two substeps of lengths ξs and $(1-\xi)s$, where the number ξ is chosen at random between 0 and 1. This *random hinge method* (see, for example, papers by Kawrakow and Bielajew [5] and Fernandez-Varea et al. [4]) can be shown (see Larsen [13]) to increase the accuracy in CH modeling. However, even these improved algorithms suffer ultimately from the lack of exact knowledge of the spatial distribution of radiation. Of equal importance for the computational success of such models, special strategies are often needed in order to deal with model inaccuracies near abrupt changes in material properties and at external boundaries, adding further to the cost of their implementation.

Larsen and Tolar have developed so-called moment condensed history (MCH) methods that improve upon the accuracy of the CCH model by preserving first and second-order spatial moments of the solution. These methods make use of the Lewis theory of moments whose main features we now outline.

Beginning with the RTE for an infinite homogeneous medium, the idea is to expand the RTE solution in spherical harmonics whose coefficients are the space-angle moments of the solution. Accuracy can then be controlled in the CH model by ensuring that low-order moments in this expansion are preserved in the approximate model. This strategy, in turn, offers the hope that a rigorous error analysis might be based on a careful analysis of the terms in the expansion that are *not* preserved by the approximate solution.

To illustrate these derivations, consider an infinite, homogeneous medium of tissue, and let the RTE solution be described by the radiation field, or radiance, $\Phi = \Phi(r,\omega,s)$ that is, in general, a function of the position $r = (x,y,z)$, direction $\omega = (\omega_x,\omega_y,\omega_z)$ and a timelike parameter s. The parameter s measures the distance travelled in a single flight in the unit direction ω along the ray between r' and r, so that $r = r' + s\omega$. Specifically, the parametrized function Φ satisfies the RTE

$$\frac{\partial\Phi(r,\omega;s)}{\partial s} + \omega\cdot\nabla\Phi + \sigma_t\Phi(r,\omega;s) = \int_{4\pi}\sigma_s f(\omega\cdot\omega')\Phi(r,\omega';s)\,d\omega'. \tag{1}$$

Here $\sigma_t = \sigma_a + \sigma_s$ is the total attenuation coefficient in tissue (=inverse of mean free path), σ_a is the absorption coefficient, σ_s is the scattering coefficient, f is the single scattering phase function = probability density function for scattering from direction ω' to ω in a single interaction. For ease of exposition, we specialize the RTE (1) to planar geometry and assume that initially each particle starts at $r = (0,0,0)$ and moves along the positive z-axis, which also serves as the north pole for a spherical coordinate system that will be used to characterize the unit direction vectors ω, ω'. That is

$$\Phi(r,\omega;0) = \frac{\delta(r)\delta(\mu-1)}{2\pi}, \tag{2}$$

where $\mu = \cos(\theta)$, and θ is the angle between the direction of travel and the positive z-axis. Under these conditions, (1) and (2) simplify to

$$\frac{\partial \Phi(z,\mu;s)}{\partial s} + \mu \frac{\partial \Phi}{\partial z} + \sigma_t \Phi(z,\mu;s) = \int_{-1}^{1} \sigma_s f_{pl}(\mu',\mu)\Phi(z,\mu';s)\,d\mu' \tag{3}$$

with the initial condition

$$\Phi(z,\mu,0) = \delta(z)\delta(\mu-1). \tag{4}$$

The derivation of (3) can be found, for example, in [14,23]; for completeness here we include it in Appendix A.

Next we expand f in the series of Legendre polynomials, P_n

$$f_{pl}(\mu',\mu) = \sum_{n=0}^{\infty} \frac{2n+1}{2} f_n P_n(\mu) P_n(\mu').$$

The zeroth-order spatial moment is obtained by integrating (3) and (4) with respect to z

$$\Phi_0(\mu,s) \equiv \int_{-\infty}^{\infty} \Phi(z,\mu;s)\,dz,$$

which produces the following equation (assuming that Φ vanishes at infinity):

$$\frac{\partial \Phi_0(\mu,s)}{\partial s} + \sigma_t \Phi_0(\mu,s) = \sum_{n=0}^{\infty} \frac{2n+1}{2} \sigma_{sn} P_n(\mu) \int_{-1}^{1} P_n(\mu')\Phi_0(\mu',s)\,d\mu' \tag{5}$$

with initial condition $\Phi_0(\mu,0) = \delta(\mu-1)$, where $\sigma_{sn} = \sigma_s f_n$. Using the orthogonality of the P_n, it can be shown that the solution of (5) is

$$\Phi_0(\mu,s) = \sum_{n=0}^{\infty} \frac{2n+1}{2} P_n(\mu) \exp(-\sigma_{an} s), \tag{6}$$

where $\sigma_{an} = \sigma_t - \sigma_{sn}$. The function $\Phi_0(\mu,s)$ is the Goudsmit–Saunderson probability density function[2] that describes the conditional probability for scattering through an angle whose cosine is μ, conditioned by having travelled a distance s and then scattered. It is used in implementations of the CCH model to sample scattering angles after travelling a user-supplied distance s.

The space-angle moment of Φ (of order n,m) is defined as

$$\Phi^{n,m}(s) = \int_{-\infty}^{\infty} \int_{-1}^{1} z^n \mu^m \Phi(z,\mu;s)\,d\mu\,dz.$$

We observe that the zeroth space-angle moment of the radiance,

$$\Phi^{0,0}(s) \equiv \int_{-1}^{1} \int_{-\infty}^{\infty} \Phi(z,\mu;s)\,dz\,d\mu = \exp(-\sigma_{a,0} s)$$

is a function of $\sigma_{a,0}$ and s only.

The theoretical foundation of the CH method is the following result: for infinite homogeneous media the space-angle moments of the radiance of total order $n+m$, $\Phi^{n,m}(s)$, depend *only* on s, the optical properties and the angular moments f_i of the phase function for $i = 0,1,\ldots,n+m$. It is this result that we refer to as the Lewis–Larsen theory [17] of moments. For completeness, we present the derivation of this result for planar geometry in Appendix B.

The Lewis–Larsen theory suggests that the key to preserving space-angle moments of the radiance is to ensure that sufficiently many angular moments of the single-scattering phase function are preserved. Below

[2] In the literature f_{GS} is often called Goudsmit–Saunderson *distribution*, even though it is a probability *density* function.

we outline how the moment condensed history (MCH) algorithm suggested in [7] makes use of the Lewis–Larsen theory. Let

$$\Phi_1(\mu, s) \equiv \int_{-\infty}^{\infty} z\Phi(z, \mu; s)\,\mathrm{d}z.$$

The function Φ_1 can be found from the differential equation

$$\frac{\partial\Phi_1(\mu, s)}{\partial s} + \sigma_t\Phi_1(\mu, s) = \mu\Phi_0(\mu, s) + \sum_{n=0}^{\infty}\frac{2n+1}{2}\sigma_{sn}P_n(\mu)\int_{-1}^{1}P_n(\mu')\Phi_1(\mu', s)\,\mathrm{d}\mu'$$

with initial condition $\Phi_1(\mu, 0) = 0$. Now the mean position for photons that have travelled a total distance s and are moving in a direction characterized by μ is

$$\bar{z}(\mu, s) = \frac{\int_{-\infty}^{\infty} z\Phi(z, \mu; s)\,\mathrm{d}z}{\int_{-\infty}^{\infty}\Phi(z, \mu; s)\,\mathrm{d}z} \tag{7}$$

with a similar definition for the second-order spatial moment, which determines the variance in the mean position, $\sigma_{\bar{z}}^2(\mu, s)$. Preservation of these two moments in the MC simulation leads to an improved MCH model [7]. In the MC simulation that implements this model, intercollision distances are based on a user-specified step size, s, and the direction of flight is sampled, as before, from the Goudsmit–Saunderson distribution. The particle is then moved to a position that is sampled from a Gaussian distribution with mean $\bar{z}(\mu, s)$ and variance $\sigma_{\bar{z}}^2(\mu, s)$. Numerical evidence reported in [7] indicates that the resulting MCH model is considerably more accurate than the original CCH.

For more general geometries, a coupled system of partial differential equations for the space-angle moments replaces (3) and could, in principle, be used to solve for the means and variances in the x-, y- and z-coordinates. Unfortunately, the resulting expressions are given by infinite series reminiscent of the series representation for the Goudsmit–Saunderson distribution [7] and so impose a heavy computational burden. Thus, while the MCH models should be considerably more accurate than the CCH model, there appears to be no easy way to use them to gain the necessary advantage in speed of execution since the cost of sampling both angle and position from the infinite series that define their distributions is high. As well, the non-stochastic determination of intercollision distances continues to impose additional computational penalties when particles cross internal interfaces and near external boundaries. The next section discusses models that address these defects.

4. Improved models: transport condensed history (TCH) methods

The developments in CH modeling of most interest to us here are also based on the Lewis–Larsen theory [6,8]. However, in contrast to the MCH models, these lead to CH algorithms that restore the random nature of the intercollision distances and produce models that satisfy transport equations that approximate the RTE for the original problem in a rather precise way.

The details of the derivations involved in the TCH model may be found in [8,15]. To summarize them here, we again begin with Eq. (1), which we rewrite as

$$\frac{\partial\Phi(r, \omega; s)}{\partial s} + \omega\cdot\nabla\Phi + (\sigma_a + \sigma_s)\Phi(r, \omega; s) = \int_{4\pi}\sigma_s f(\omega\cdot\omega')\Phi(r, \omega'; s)\,\mathrm{d}\omega' \tag{8}$$

with the same boundary conditions (2). Once again expanding the single scattering phase function f in Legendre polynomials, and rearranging, (8) may be rewritten

$$\frac{\partial\Phi(r, \omega; s)}{\partial s} + \omega\cdot\nabla\Phi + \sigma_a\Phi(r, \omega; s) = -\sum_{n=0}^{\infty}\frac{2n+1}{4\pi}\left(\frac{1-f_n}{\lambda}\right)\int_{4\pi}P_n(\omega\cdot\omega')\Phi(r, \omega'; s)\,\mathrm{d}\omega', \tag{9}$$

where $\lambda = \frac{1}{\sigma_s}$ is the scattering mean free path in the medium. Now by introducing a parameter called the excess mean free path, λ_s and constants $a_n(\lambda_s)$ that depend on it by means of the equation

$$\frac{1-f_n}{\lambda}=\frac{1-a_n(\lambda_s)}{\lambda+\lambda_s},\quad \lambda\geqslant 0$$

the equation

$$\frac{\partial\Phi(r,\omega;s)}{\partial s}+\omega\cdot\nabla\Phi+\sigma_a\Phi(r,\omega;s)+\frac{1}{\lambda+\lambda_s}\Phi(r,\omega;s)=\frac{1}{\lambda+\lambda_s}\int_{4\pi}f_{\lambda_s}(\omega\cdot\omega')\Phi(r,\omega';s)\,d\omega' \tag{10}$$

where

$$f_{\lambda_s}(\omega\cdot\omega')=\sum_{n=0}^{\infty}\frac{2n+1}{4\pi}a_n(\lambda_s)P_n(\omega\cdot\omega')$$

replaces (9) and is algebraically identical to it. This equation incorporates an enlarged scattering mean free path $\lambda+\lambda_s$ that approaches the original scattering mean free path λ as the excess mean free path, λ_s, approaches 0. It would be ideal to use (10) as a basis of a CH model except for the fact that the new single scattering phase function $f_{\lambda_s}(\omega\cdot\omega')$ is not, in general, nonnegative and so may not be used as it stands as a probability density function for sampling directions after scattering. The idea used in [15] to circumvent this flaw is to replace the function f_{λ_s} by a legitimate probability density function F_{λ_s}, thus making the new equation

$$\frac{\partial\Phi(r,\omega;s)}{\partial s}+\omega\cdot\nabla\Phi+\sigma_a\Phi(r,\omega;s)+\frac{1}{\lambda+\lambda_s}\Phi(r,\omega;s)=\frac{1}{\lambda+\lambda_s}\int_{4\pi}F_{\lambda_s}(\omega\cdot\omega')\Phi(r,\omega';s)\,d\omega'$$

an RTE that can be simulated as a true transport process with an increased scattering mean free path. This device completely obviates the need to use special boundary and interface crossing strategies to overcome model inaccuracies in those portions of phase space, a distinct advantage. Furthermore, Tolar has selected the function F_{λ_s} in such a way that the resulting transport process converges to the original transport process as the excess mean free path tends to 0. Numerical results reported in [8,15] are impressive and this TCH algorithm appears to be a useful technique potentially for modeling both electron and photon transport. However, the mechanisms employed in [8,15] only preserve the first two moments of the original scattering process so that, even for an infinite medium, second-order quantities like the standard deviation about mean locations will be simulated inaccurately. Tolar also shows that the truncation error associated with the TCH algorithm as presented in his dissertation [15] is $O(\lambda_s)$. Ideally, higher-order accuracy would be very desirable.

In the next two sections, we describe other TCH models that use somewhat different approaches to taking advantage of the Lewis–Larsen theory. In both of these cases, as we shall see, the idea is once again to alter both the mean free path and the scattering properties to speed up the computation without sacrificing too much accuracy. However, the order of selection will be reversed: we will *first* identify a new scattering phase function that preserves a predetermined number of angular moments, and this choice will *determine* the increase in mean free path that is possible in the model. Pursuing this approach guarantees that the scattering phase function is non-negative everywhere and that the increase in mean free path is the largest possible that is consistent with the new scattering law.

5. Similarity theory (ST model)

This CH type algorithm for efficient simulation of photon transport was developed by Wyman et al. [9]; we outline their derivation below.

We begin with the RTE for the photon density, or radiance Φ in the time-independent case

$$\omega\cdot\nabla\Phi+\sigma_t\Phi=\int_{4\pi}\sigma_s f_{HG}(\omega\cdot\omega')\Phi(r,\omega')\,d\omega'+Q(r,\omega) \tag{11}$$

which, together with appropriate boundary and initial conditions, characterizes the problem. In (11), Q defines a possible internal volumetric source and, because our interest now narrows to the treatment of photon transport in tissue, we make use of the Henyey–Greenstein single scattering phase function, f_{HG}, traditionally used to model scattering of light in tissue

$$f_{\mathrm{HG}}(\mu_0) = \frac{1}{2\pi}\frac{1-g^2}{2(1-2g\mu_0+g^2)^{3/2}},$$

where $\mu_0 = \omega\cdot\omega'$ and g is a parameter chosen to describe anisotropy

$$g = \int_{-1}^{1} \mu_0 f_{\mathrm{HG}}(\mu_0)\,\mathrm{d}\mu_0.$$

(see Appendix A for additional detail). To proceed, we rewrite Eq. (11) combining the terms containing tissue optical properties into one term $I(r,\omega)$,

$$\omega\cdot\nabla\Phi - Q(r,\omega,t) + I(r,\omega) = 0, \tag{12}$$

where

$$I(r,\omega) = \sigma_{\mathrm{t}}\Phi(r,\omega) - \int_{4\pi}\sigma_{\mathrm{s}} f_{\mathrm{HG}}(\omega\cdot\omega')\Phi(r,\omega')\,\mathrm{d}\omega'. \tag{13}$$

It is now clear that one can substitute altered optical coefficients, σ_{a}^*, σ_{s}^* and a new phase function f^* in (12) without affecting the solution as long as the quantity I remains unchanged. This leads to the similarity relations requirement:

$$[(\sigma_{\mathrm{a}}-\sigma_{\mathrm{a}}^*) + (\sigma_{\mathrm{s}}-\sigma_{\mathrm{s}}^*)]\Phi(r,\omega,t) = \int_{4\pi}\Phi(r,\omega',t)[\sigma_{\mathrm{s}} f_{\mathrm{HG}}(\omega\cdot\omega') - \sigma_{\mathrm{s}}^* f^*(\omega\cdot\omega')]\,\mathrm{d}\omega'. \tag{14}$$

Upon expanding the radiance and phase functions in spherical harmonics, using orthogonality and the addition theorem for Legendre polynomials, one arrives at the following system of equations:

$$[(\sigma_{\mathrm{a}}-\sigma_{\mathrm{a}}^*) + \sigma_{\mathrm{s}}(1-f_n) - \sigma_{\mathrm{s}}^*(1-f_n^*)] = 0, \quad n = 0,1,\ldots, \tag{15}$$

which can also be written

$$I_n \equiv \sigma_{\mathrm{t}} - \sigma_{\mathrm{s}} f_n = \sigma_{\mathrm{t}}^* - \sigma_{\mathrm{s}}^* f_n^* \equiv I_n^*, \quad n = 0,1,\ldots, \tag{16}$$

where f_n, f_n^* are the Legendre moments of f_{HG}, f^*, respectively. The quantities I_n combine the optical properties of the medium and the properties of the scattering phase function. We will call I_n the nth *optical invariant*; these quantities characterize the solution and contain the information required for the simulations. The CH modeling approach that we take in this paper relies on preserving a certain number, $S+1$, of the optical invariants of the exact model

$$I_n = I_{n,\mathrm{CH}}, \quad n = 0,\ldots,S. \tag{17}$$

Note that since both f and f^* are density functions, we must have $f_0 = f_0^* = 1$ and thus $\sigma_{\mathrm{a}} = \sigma_{\mathrm{a}}^*$ in (15). This implies that the system (15) is trivially satisfied for $n = 0$. Truncating the system (15) at $n = S$ then provides S additional equivalence relations

$$\frac{\sigma_{\mathrm{s}}^*}{\sigma_{\mathrm{s}}} = \frac{1-f_n}{1-f_n^*}, \quad n = 1,\ldots,S \tag{18}$$

called *similarity relations of order S*. Note also that the system (18) is underdetermined: it has S equations and $S+1$ unknowns: f_1^* through f_S^* and σ_{s}^*. To make this system uniquely solvable, one usually assumes that $f_S^* = 0$.

The system of Eq. (18) suggests that we are free to choose the new scattering law incorporated in σ_{s}^* and f^*, as long as they satisfy these similarity relations; that is, as long as they leave the optical invariants unchanged. We would like to choose these new parameters in such a way that the particle intercollision distances increase. The particle intercollision distance, or mean free path (mfp), is $1/\sigma_{\mathrm{t}}$ and in tissue, often absorption is small relative to scattering so $1/\sigma_{\mathrm{t}}^* \approx 1/\sigma_{\mathrm{s}}^*$. Thus, we would like to choose σ_{s}^* to be as small as possible. Also, we want to select S, the order of the similarity relation, as large as possible, in order to achieve good accuracy.

By assumption, $f_S^* = 0$ and for f_{HG} we have: $f_n = g^n$, therefore the new scattering cross-section becomes $\sigma_{\mathrm{s}}^* = \sigma_{\mathrm{s}}(1-g^S)$. Since $g^S \to 0$ as $S\to\infty$, we see that $\sigma_{\mathrm{s}}^* \to \sigma_{\mathrm{s}}$ as $S\to\infty$. This also follows from the uniqueness

of the RTE solution: as the degree, S, of the approximation increases we are led back to the original solution. Thus, there is a trade-off between accuracy and speed when applying the similarity relations.

For a given S the expected speed-up in the Monte Carlo simulation can be estimated by the ratio of mean free paths, $\frac{1/\sigma_s^*}{1/\sigma_s} = \frac{1}{1-g^S}$ while the accuracy of the method is determined by S: similarity relations of order S preserve $M = S + 1$ optical invariants.

Now with σ_s^* given by $\sigma_s^* = \sigma_s(1 - g^S)$, one can solve the system (18) for f_n^*, $n = 1, \ldots, S-1$. To implement the simulation, we could reconstruct f^* according to its Legendre expansion. To simplify the sampling from f^*, the authors [9] defined f^* as a linear combination of orthogonal step functions on $[-1, 1]$, constructed using Legendre polynomials. We describe our implementation of this construction for orders $S = 2, 4, 12$ in Section 8.

6. Discrete scattering angles (DSA model)

For electron transport, Prinja and Franke [10] suggested seeking an approximation to the scattering phase function in the form of a linear combination of delta functions chosen to preserve the momentum transfer moments

$$\xi_n \equiv \int_{-1}^{1} (1 - \mu_0)^n f(\mu_0)\, \mathrm{d}\mu_0, \quad n = 0, 1, \ldots \tag{19}$$

corresponding to the single scattering phase function f. This choice was motivated by the highly forward-peaked nature of electron scattering: since μ_0, on average, is very close to 1, one might expect that $\{\xi_n\}_{n=0}^{\infty}$ converges rapidly to 0. Hence an approximate phase function that preserves only a few of the momentum transfer moments should be a good approximation to the exact phase function. However, the precise behavior of the momentum transfer moments as n increases depends very sensitively on the specific description of the single scattering function f. For example, the Henyey–Greenstein phase function, f_{HG}, is such that even when the average cosine g of the scattering angle μ_0 is close to 1 (but not equal to 1) its momentum transfer coefficients, ξ_n *do not* decrease with increasing n [16,17]. Indeed, the merit of each CH method requires a more careful analysis than intuitively based arguments can provide. Our approach to this crucial issue is described in Section 9.

We use the ideas of Sloan [18] to approximate the phase function by a set of discrete scattering angles that are chosen to preserve the *regular* Legendre moments of $f \equiv f_{\mathrm{HG}}$, but with the *proviso* that one of the angles is pre-assigned to be equal to zero, corresponding to $\mu = 1$

$$f_{\mathrm{d}}(\mu_0) = \sum_{i=1}^{D-1} w_i \delta(\mu_0 - \mu_i) + w_D \delta(\mu_0 - 1) \tag{20}$$

with $w_D \neq 0$. The weights $w_i,\ i = 1, \ldots, D$ and scattering cosines $\mu_i,\ i = 1, \ldots, D-1$ in (20) are then found by requiring that the $2D - 1$ angular moments taken with respect to f_{d} and with respect to the exact phase function, f_{HG}, are equal to each other

$$M_k \equiv \int_{-1}^{1} \mu_0^k f_{\mathrm{HG}}(\mu_0)\, \mathrm{d}\mu_0 = \int_{-1}^{1} \mu_0^k f_{\mathrm{d}}(\mu_0)\, \mathrm{d}\mu_0, \quad k = 0, \ldots, 2D-2. \tag{21}$$

The representation (20) identifies a forward-peaked component of scattering in the term $w_D\delta(\mu_0 - 1)$ and uses the remaining constraints to correct for this exaggeration of the $\mu_0 = 1$ term. Since scattering in the forward $\mu_0 = 1$ direction amounts to no scattering at all in the simulation, the remaining terms prescribe scattering that is much more isotropic. The increased mean free path can be determined exactly from (20), as will be seen shortly.

Wyman and Patterson [19] also attempted to represent their phase function as a linear combination of delta spikes. Rather than solving the non-linear system (21), however, those authors pre-assign the spike locations, μ_i, and solve the resulting linear system for the spike amplitudes, w_i. This approach often resulted in negative weights, w_i, when the number of discrete angles exceeded four. Sloan [18] pointed out that the use of Gauss–Radau quadrature method eliminates this flaw. That is, all discrete scattering angles determined by the Gauss–

Radau prescription have cosines μ_0 that satisfy $-1 \leqslant \mu_0 \leqslant 1$, and the associated weights must also be positive when the Gaussian weight function is nonnegative, as in our case [21].

We note that preserving regular moments in the sense of (21) is equivalent to preserving Legendre moments of f_{HG}, as well as momentum transfer moments, since any monomial of degree k can be represented as a finite sum of Legendre polynomials up to order k. Since, as we remarked earlier, scattering with $\mu_0 = 1$ is equivalent, from the simulation point of view, to no scattering at all, we can simply sample the scattering angle from $f^*(\mu_0) = \sum_{i=1}^{D-1} w_i \delta(\mu_0 - \mu_i)/\sum_{i=1}^{D-1} w_i$. The weight w_D associated with $\mu_0 = 1$ then determines how much the mean free path increases and hence, the saving in time of computation.

Consider again the time-independent RTE for the radiance

$$\omega \cdot \nabla \Phi + \sigma_{\mathrm{t}} \Phi = \sigma_{\mathrm{s}} \int_{4\pi} f_{\mathrm{HG}}(\omega \cdot \omega') \Phi(r, \omega') \, \mathrm{d}\omega' + Q(r, \omega). \tag{22}$$

Making use of the derivation in Appendix A again, we can write the integral in (22) as

$$\sigma_{\mathrm{s}} \int_{4\pi} f_{\mathrm{HG}}(\omega \cdot \omega') \Phi(r, \omega') \, \mathrm{d}\omega' = \frac{\sigma_{\mathrm{s}}}{2\pi} \int_{4\pi} f_{\mathrm{HG}}(\mu_0) \Phi(r, \omega') \, \mathrm{d}\omega' = \frac{\sigma_{\mathrm{s}}}{2\pi} \int_0^{2\pi} \int_{-1}^{1} f_{\mathrm{HG}}(\mu_0) \Phi(r, \omega') \, \mathrm{d}\mu' \, \mathrm{d}\varphi'. \tag{23}$$

Upon substituting Eq. (20) for f_{d} in place of f_{HG} in (23), the integral becomes

$$\begin{aligned} \int_0^{2\pi} \int_{-1}^{1} f_{\mathrm{HG}}(\mu_0) \Phi(r, \omega') \, \mathrm{d}\mu' \, \mathrm{d}\varphi' = & \int_0^{2\pi} \int_{-1}^{1} \sum_{i=1}^{D-1} w_i \delta(\mu_0 - \mu_i) \Phi(r, \omega') \, \mathrm{d}\mu' \, \mathrm{d}\varphi' \\ & + \int_0^{2\pi} \int_{-1}^{1} w_D \delta(\mu_0 - 1) \Phi(r, \omega') \, \mathrm{d}\mu' \, \mathrm{d}\varphi'. \end{aligned} \tag{24}$$

The second term in (24) can be simplified since $\mu_0 = 1$ implies that $\omega' = \omega$

$$\int_0^{2\pi} \int_{-1}^{1} w_D \delta(\mu_0 - 1) \Phi(r, \omega') \, \mathrm{d}\mu' \, \mathrm{d}\varphi' = \int_0^{2\pi} w_D \Phi(r, \omega) \, \mathrm{d}\varphi' = 2\pi w_D \Phi(r, \omega). \tag{25}$$

Thus, (22) becomes

$$\omega \cdot \nabla \Phi + \sigma_{\mathrm{t}} \Phi = \frac{\sigma_{\mathrm{s}}}{2\pi} \int_{4\pi} \sum_{i=1}^{D-1} w_i \delta(\mu_0 - \mu_i) \Phi(r, \omega') \, \mathrm{d}\omega' + \sigma_{\mathrm{s}} w_D \Phi(r, \omega) + Q(r, \omega). \tag{26}$$

The function that replaces the original phase function under the integral sign in (26) must be re-normalized so that it remains a probability density function. Upon rearranging terms and re-normalizing we obtain

$$\omega \cdot \nabla \Phi + \sigma_{\mathrm{a}} \Phi + \sigma_{\mathrm{s}}[1 - w_D] \Phi = \sigma_{\mathrm{s}} \left[\sum_{i=1}^{D-1} w_i \right] \frac{1}{2\pi} \int_{4\pi} \frac{\sum_{i=1}^{D-1} w_i \delta(\mu_0 - \mu_i)}{\sum_{i=1}^{D-1} w_i} \Phi(r, \omega') \, \mathrm{d}\omega' + Q(r, \omega). \tag{27}$$

It follows from (21) that for $k = 0$ we have $\sum_{i=1}^{D} w_i = 1$, so we can rewrite Eq. (27) as

$$\omega \cdot \nabla \Phi + \sigma_{\mathrm{a}} \Phi + \sigma_{\mathrm{s}}[1 - w_D] \Phi = \sigma_{\mathrm{s}}[1 - w_D] \frac{1}{2\pi} \int_{4\pi} \frac{\sum_{i=1}^{D-1} w_i \delta(\mu_0 - \mu_i)}{[1 - w_D]} \Phi(r, \omega') \, \mathrm{d}\omega' + Q(r, \omega). \tag{28}$$

Since (28) has the same algebraic form as the starting Eq. (22), the quantity $\sigma_{\mathrm{s}}[1 - w_D]$ in Eq. (28) can be interpreted as the new scattering cross-section, σ_{s}^*, and we can select intercollision distances for this CH model according to the exponential distribution with mean $1/\sigma_{\mathrm{s}}^*$. From the expression $\sigma_{\mathrm{s}}^* = \sigma_{\mathrm{s}}[1 - w_D]$ we see that the more forward-peaked the original phase function, the more the intercollision distance can be stretched. The expected speed-up of such a simulation is estimated by the ratio $\frac{1/\sigma_{\mathrm{s}}^*}{1/\sigma_{\mathrm{s}}} = \frac{1}{1 - w_D}$.

7. Evaluating CH models

In this section we compare the theoretical accuracy of the DSA and ST models. By construction, the phase function with D discrete angles

$$f_{\mathrm{d}}(\mu_0) = \sum_{i=1}^{D-1} w_i \delta(\mu_0 - \mu_i) + w_D \delta(\mu_0 - 1) \tag{29}$$

has its first $2D-1$ Legendre moments equal to the corresponding Legendre moments of the original single scattering phase function, f_{HG}

$$\int_{-1}^{1} P_n(\mu_0) f_{\mathrm{d}}(\mu_0)\,\mathrm{d}\mu = \sum_{i=1}^{D-1} w_i P_n(\mu_i) + w_D = g^n, \quad n = 0, \ldots, 2D-2. \tag{30}$$

With the phase function f^* used in the simulation in place of (29), where

$$f^*(\mu_0) = \frac{\sum_{i=1}^{D-1} w_i \delta(\mu_0 - \mu_i)}{1 - w_D} \tag{31}$$

the new scattering cross-section becomes: $\sigma_{\mathrm{s}}^* = \sigma_{\mathrm{s}}(1 - w_D)$. The nth Legendre moment of f^*, f_n^*, is then

$$f_n^* = \int_{-1}^{1} P_n(\mu_0) f^*(\mu_0)\,\mathrm{d}\mu = \frac{\sum_{i=1}^{D-1} w_i P_n(\mu_i)}{1 - w_D}, \quad n = 0, 1, 2, \ldots. \tag{32}$$

From (30) and (32) it follows that for $n = 0, \ldots, 2D-2$:

$$f_n^* = \frac{g^n - w_D}{1 - w_D}, \qquad \sigma_{\mathrm{s}}^* = \sigma_{\mathrm{s}}(1 - w_D) \tag{33}$$

and thus the familiar system of equations derived for similarity of order S

$$\sigma_{\mathrm{s}}(1 - g^n) = \sigma_{\mathrm{s}}^*(1 - f_n^*), \quad n = 0, \ldots, S$$

for the f_n^* and σ_{s}^* given by (33), is satisfied for $n = 0, \ldots, 2D-2$, since

$$\sigma_{\mathrm{s}}^*(1 - f_n^*) = \sigma_{\mathrm{s}}(1 - w_D)\left[1 - \frac{g^n - w_D}{1 - w_D}\right] = \sigma_{\mathrm{s}}(1 - g^n). \tag{34}$$

We conclude that the DSA model with D distinct scattering directions, including the directly forward direction, has similarity order $S = 2D-2$ and therefore should be roughly twice as accurate as the similarity relation of order D which preserves only $D+1$ optical invariants in infinite homogeneous media.

For the numerical results presented in Section 9 we chose the orders of the ST and DSA methods, S and D, respectively, so that the methods preserve the *same* number M of optical invariants. We picked the values shown in Table 1.

Our interest in this paper on problems in biomedical optics that model light-tissue interactions motivates us to test our candidate CH models on highly simplified photon transport problems. For this purpose, we study a volume of homogenous tissue in three-dimensional slab geometry with a source of light impinging on the $z = 0$ surface. We are interested in estimating the amount of light that is either reflected or transmitted from such a slab when the slab thickness is a large number of optical mean free paths. For our study we chose the following optical properties typical of tissue: $\sigma_{\mathrm{s}} = 0.994466,\ \sigma_{\mathrm{a}} = 0.0055,\ \sigma_{\mathrm{t}} = 1,\ g = 0.9$, and we set the length of the slab L for the largest problem we studied to 100 mfp.

The propagation of light in the absence of internal volumetric sources is governed generally by the time-independent RTE

Table 1
Selected CH orders and the corresponding number of optical invariants

S	D	M
2	2	3
4	3	5
12	7	13

S = similarity order, D = number of discrete scattering cosines, M = number of optical invariants preserved.

$$\omega \cdot \nabla \Phi(r,\omega) + \sigma_t \Phi(r,\omega) = \int_{4\pi} \sigma_s f_{HG}(\omega \cdot \omega') \Phi(r,\omega')\, d\omega',$$

where we have assumed a homogeneous medium with known optical properties σ_s, σ_a, g and specialized again to the Henyey–Greenstein scattering law, f_{HG}. Focusing on slab geometry, where the tissue ranges from $z = 0$ to $z = L$, we add the boundary conditions

$$\Phi(x,y,0,\mu_0) = Q_0, \quad 0 < \mu_0 \leqslant 1,$$
$$\Phi(x,y,L,\mu_0) = 0 \quad -1 \leqslant \mu_0 < 0,$$

corresponding to a light source at the $z = 0$ end of the slab directed inward, with no source at the $z = L$ end. The problem we would like to solve is to estimate the amounts of light reflected and transmitted, R and T, respectively, by Monte Carlo simulation.

We will solve this prototype problem in several different ways for the purpose of making meaningful comparisons of the results obtained using our proposed CH models with those obtained by conventional Monte Carlo simulation. For all of our simulations, we modeled light absorption by a continuously varying photon weight [20]. This weight, initially unity, is reduced by a factor of $\exp(-\sigma_a l)$ when the photon travels a distance l, where the intercollision distances l are distributed exponentially with mean $1/\sigma_s$. This means that if the weight of a photon leaving a collision is W_0, and it travels a distance l before arriving at the next collision point, the arriving weight is $W_1 = W_0 \exp(-\sigma_a l)$ and the complementary weight, $W_2 = W_0(1 - \exp(-\sigma_a l))$ has been allocated to absorption along the track of length l.

8. Three implementations

8.1. Analog Monte Carlo

We processed 10^6 photon biographies and tallied their weights upon either being reflected or transmitted from 100 mean free paths of tissue with the optical parameters described above. The Henyey–Greenstein scattering phase function was sampled to determine a new direction following each scattering interaction. Since absorption of light internal to the tissue is not allowed to terminate the photon history, every biography processed leads ultimately either to transmission or reflection. The averages of the weights transmitted and reflected, and their standard deviations, provide the estimates of R and T for this analog simulation.

8.2. Similarity theory

As we described in Section 5, this method is implemented by replacing the Henyey–Greenstein function with a new scattering law based on a phase function f^* and a scattering coefficient, σ_s^*, in such a way that the similarity relations (18) are satisfied. We mimicked the construction in [9] of f^* using orthogonal step functions. Our treatment of absorption through continuous weight reduction results in accurate simulation of particle transport everywhere in the tissue. This eliminates the need to supplement the ST simulation with the use of analog MC near the boundaries, as was done in [9]. For the selected optical properties the resulting altered scattering cross-sections, σ_s^*, for ST of orders 2, 4 and 12 are

S	2	4	12
$\sigma_s^* = \sigma_s(1 - g^S)$	0.1889	0.3420	0.7136

The corresponding f^* are shown in Figs. 1–3.

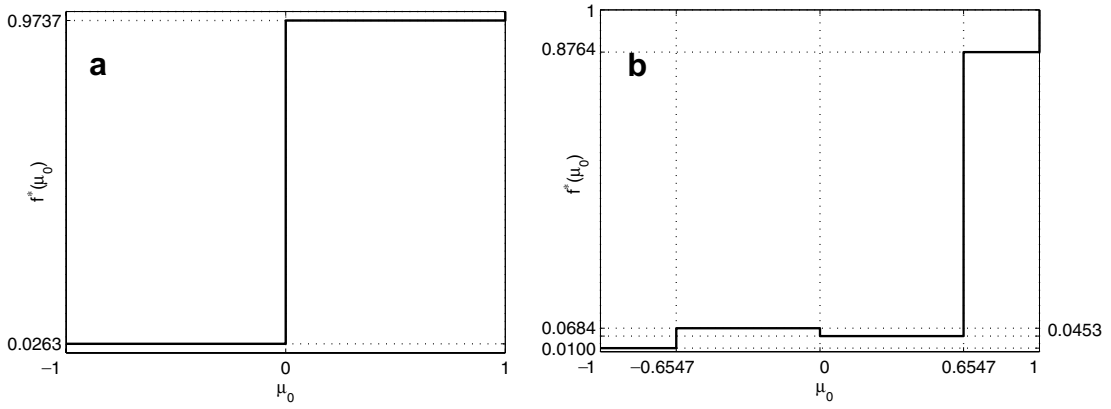

Fig. 1. $f^*(\mu_0)$ for ST: (a) $S = 2$, (b) $S = 4$.

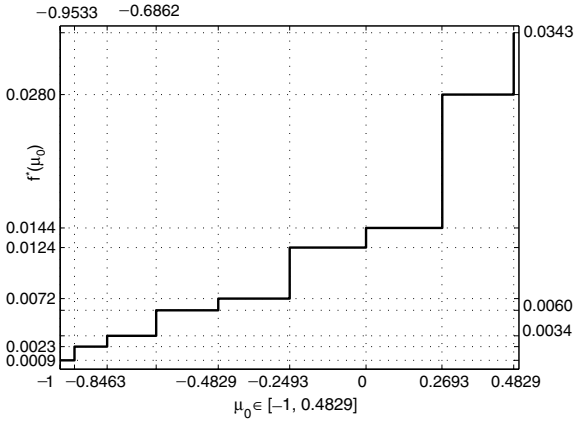

Fig. 2. $f^*(\mu_0)$ for ST, $S = 12,\ \mu_0 \in [-1, 0.48291]$.

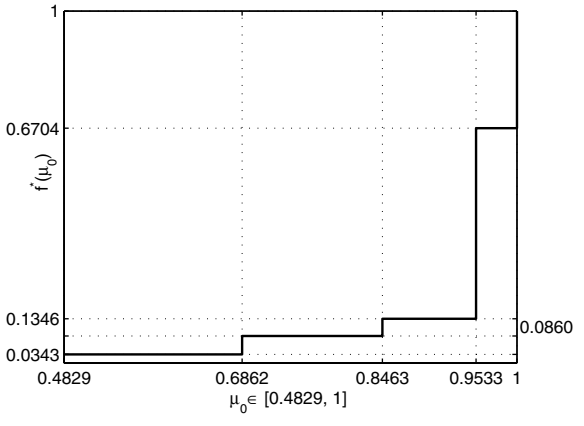

Fig. 3. $f^*(\mu_0)$ for ST, $S = 12,\ \mu_0 \in [0.4829, 1]$.

8.3. Discrete scattering angles

For this CH model, we describe scattering in terms of the probability density function f_d given by Eq. (20) making use of the distinct scattering cosines, one of which results in no change in direction. For the selected optical properties we solve the system (21) by Gauss–Radau quadrature (see [21]).

D	2	3	7
$\sigma_s^* = \sigma_s(1 - w_D)$	0.0135	0.2472	0.5271

The corresponding f^* are shown in Figs. 4 and 5.

Using 10^6 random walks for each of the 2 CH model simulations, we compare the estimates (sample means and standard deviations) of R and T obtained by analog Monte Carlo with the estimates obtained using these two CH algorithms. These results are listed in Table 2.

We observe that the accuracy of each CH method appears to increase as the number M of optical invariants preserved increases. Also notice that for a given M, the DSA method is 40–50% faster than ST. Apart from the smaller values of σ_s^* for DSA when compared to ST, we have traced this gain primarily to the reduced cost of sampling the scattering angles in DSA.

With only 10^6 random walks processed for each method, the comparisons of accuracy displayed in Table 2 are far from conclusive. That is why we carry out additional error analysis in Section 9.

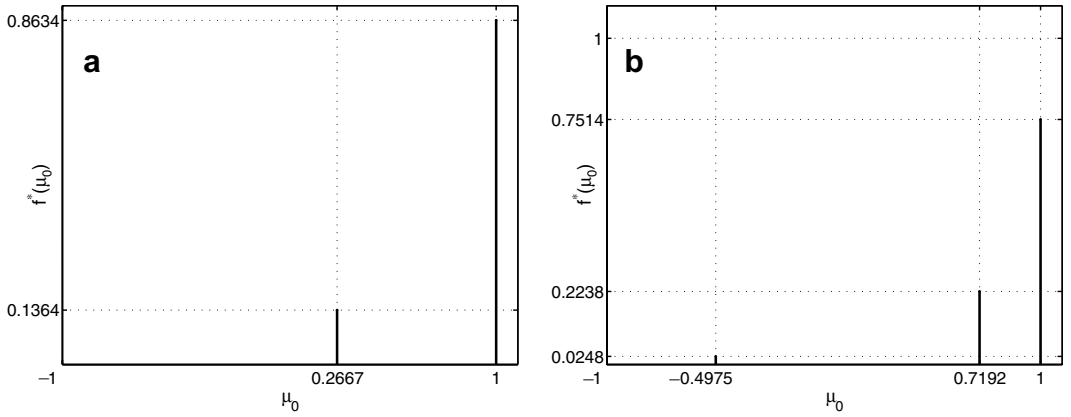

Fig. 4. $f^*(\mu_0)$ for DSA: (a) $D = 2$, (b) $D = 3$.

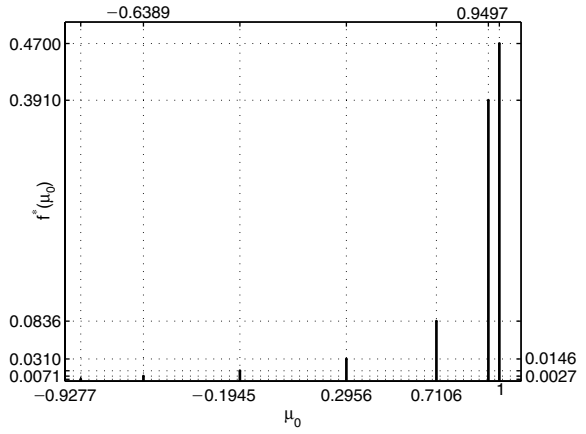

Fig. 5. $f^*(\mu_0)$ for DSA, $D = 7$.

Table 2
Comparison of reflectivity and transmissivity estimates from analog Monte Carlo (AMC), similarity theory (ST) and discrete scattering angles (DSA)

M	Method	$R \pm$ std	$T \pm$ std	time (s)
∞	AMC	$0.503295 \pm 3.6079e{-}004$	$0.013521 \pm 4.9879e{-}005$	311
3	DSA, $D = 2$	$0.500835 \pm 3.6379e{-}004$	$0.013653 \pm 5.3778e{-}005$	39
3	ST, $S = 2$	$0.501182 \pm 3.6297e{-}004$	$0.013772 \pm 5.2102e{-}005$	60
5	DSA, $D = 3$	$0.503861 \pm 3.6461e{-}004$	$0.013572 \pm 5.0982e{-}005$	77
5	ST, $S = 4$	$0.504340 \pm 3.6280e{-}004$	$0.013460 \pm 5.0632e{-}005$	109
13	DSA, $D = 7$	$0.503340 \pm 3.6246e{-}004$	$0.013481 \pm 5.0488e{-}005$	163
13	ST, $S = 12$	$0.503382 \pm 3.60996e{-}004$	$0.013512 \pm 5.0688e{-}005$	230

Table 3
Comparison of expected and observed speed gains for each CH method studied

ST speed gains: expected/observed	S	D	DSA speed gains: expected/observed
5.3/5.2	2	2	7.3/7.9
2.9/2.9	4	3	4.0/4.0
1.4/1.4	12	7	1.9/1.9

Table 4
Comparison of figures of merit for AMC, ST and DSA

	ST, $S = 4$	DSA, $D = 3$	AMC
F_R	6.9701e+004	9.7690e+004	2.4702e+004
F_T	3.5787e+006	4.9966e+006	1.2924e+006

The theory presented earlier also enables us to estimate the expected gain in speed of execution from each CH simulation by the ratio of scattering cross-sections: $\frac{1/\sigma_s^*}{1/\sigma_s}$. From Table 3 we see that the expected and the observed speed gains are in good agreement.

Finally, we define a figure of merit, F_x, from each MC simulation that produces an estimate of a quantity x through the formula: $F_x = (variance_x \cdot runtime)^{-1}$, where $variance_x$ is the variance obtained in estimating x and *runtime* measures the total elapsed computer time in obtaining this estimate. This combination of statistical uncertainty and time of execution on a single computational platform is appropriate for comparing the overall efficiency of one MC simulation method with another because F_x should be roughly independent of the number H of histories processed (since the variance should be inversely proportional to H) while *runtime* should be roughly directly proportional to H. In Table 4 we compare the figures of merit, F_R and F_T, of the two CH algorithms as well as AMC in estimating R and T, respectively, when, for example, $S = 4,\ D = 3$. We chose these values for this comparison to illustrate how CH might perform even for small S and D. A more efficient algorithm has a higher figure of merit. From Table 4 we see that the DSA method has better figures of merit than the ST method and that both improve upon AMC. We observe similar results for other values of M.

This efficiency analysis, based as it is on statistical uncertainties, does not directly address the absolute accuracies of the two CH methods. We anticipate that the accuracy of each CH algorithm is measured by the number M of optical invariants preserved. In the next section we will refine this statistically based analysis of efficiency with an analytical error analysis in order to confirm these preliminary findings.

9. Further error analysis

Because the Monte Carlo simulation comparisons discussed in the last section have statistical uncertainties that make comparisons treacherous, we seek in this section to carry our analysis of the error a step further.

For this purpose, we re-examine the idealized tissue problem equation (11) that describe transport in a semi-infinite homogeneous volume of tissue and consider the projection of the solution on the depth axis. This simplifies the analysis since the resulting radiance becomes a function of only the depth coordinate, z, and the cosine of the unit direction of travel, μ. We refer to this as the (z, μ) *problem.* Because there is no exact analytical solution of the (z, μ) problem in closed form, our strategy is to compare Nth order spherical harmonics expansions of the solutions that correspond to the true σ_s and phase function, f, and their CH substitutes, σ_s^*, f^*; denote these by Φ_N and $\Phi_{N,\mathrm{CH}}$, respectively. Solutions of the truncated spherical harmonic representation, described in the literature [14] as P_N-approximations, can be obtained by various numerical methods other than simulation and, for sufficiently large choices of the order N of approximation, can serve to reinforce further the stochastic comparative analysis of Section 8. For the analysis carried out in Sections 9.1 and 9.2, we chose $N = 16$, which produces a P_{17} solution.

9.1. (z,μ)-Problem equations

We show in Appendix A that when the idealized tissue problem equation

$$\omega \cdot \nabla \Phi + \sigma_t \Phi = \int_{4\pi} \sigma_s f_{\mathrm{HG}}(\omega \cdot \omega') \Phi(r, \omega') \, \mathrm{d}\omega' \tag{35}$$

is projected onto the z-axis, the governing equation becomes

$$\mu \frac{\mathrm{d}\Phi(z,\mu)}{\mathrm{d}x} + \sigma_t \Phi(z,\mu) = \sigma_s \int_{-1}^{1} f_{\mathrm{pl}}(\mu', \mu) \Phi(z, \mu') \, \mathrm{d}\mu', \tag{36}$$

where

$$f_{\mathrm{pl}}(\mu', \mu) = \sum_{n=0}^{\infty} \frac{2n+1}{2} g^n P_n(\mu) P_n(\mu') \tag{37}$$

with the boundary conditions

$$\begin{aligned} \Phi(0, \mu) &= Q_{0,} \quad \mu > 0, \\ \Phi(L, \mu) &= 0, \quad \mu < 0. \end{aligned}$$

In our implementation we chose to solve the P_N-equations by using the equivalent [22,23] discrete ordinates (S_N) method, whose solution is obtained by discretizing the angular variable, μ. The S_N algorithm that we implement was suggested by Gelbard [23] specifically to minimize the effect of round-off errors and produces robust solutions, even for thick slabs. Numerical solutions of the P_N equations are notoriously unstable and subject to considerable loss of precision generally, but Gelbard's analytically-based method works very well for slab geometry. Numerical stability is particularly important to us since we want to examine the differences between Φ_N and $\Phi_{N,\mathrm{CH}}$ which we expect will be very small. Thus, high accuracy and robustness with respect to growth of round-off errors are essential.

9.2. Numerical results and discussion

For the figures below we set the slab length, L, to 100 mean free paths, the number of terms in the Legendre expansion of the radiance, N, to 16 and we varied M – the number of optical invariants preserved; i.e. the number of equations satisfied in the system (16). First, in Fig. 6 we plot the differences between the optical invariants of the P_{17} model and the two CH models; i.e. we plot

$$I_n - I_n^* = \sigma_s(1 - f_n) - \sigma_s^*(1 - f_n^*), \quad n = 0, \ldots, 16.$$

In all the plots, circles represent ST method results and crosses represent DSA method results. The data shown in Fig. 6 illustrates that for a given M, the DSA parameters satisfy $2M - 1$ equations in (16) while the ST parameters satisfy only the first $M + 1$ of these equations.

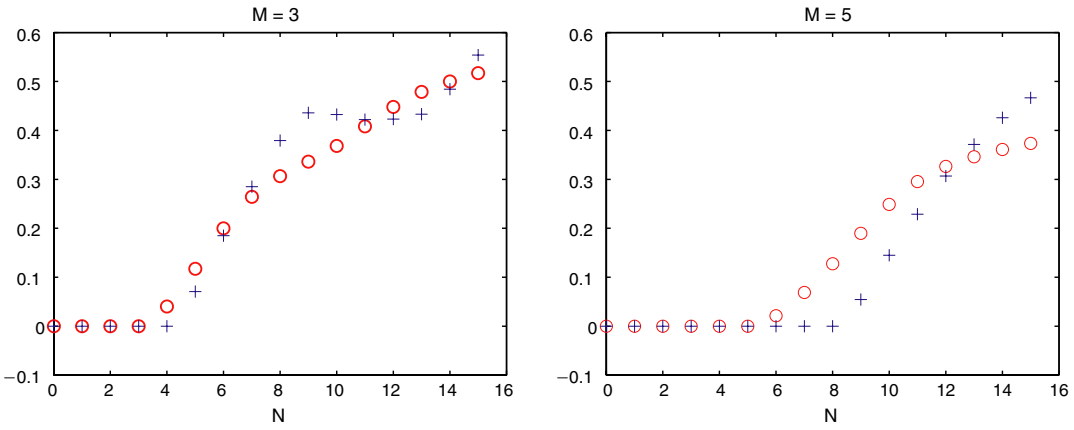

Fig. 6. Error in optical invariants, I_n.

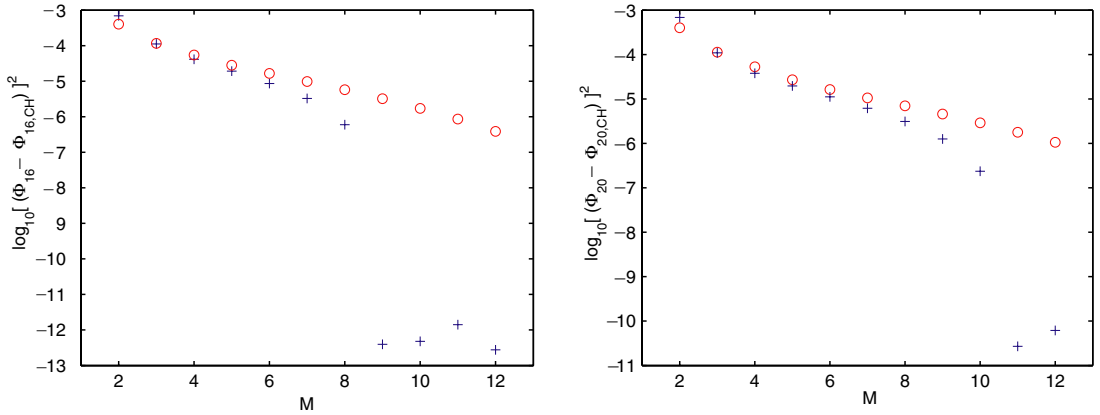

Fig. 7. Mean square errors in radiance on $\log_{10}$ scale.

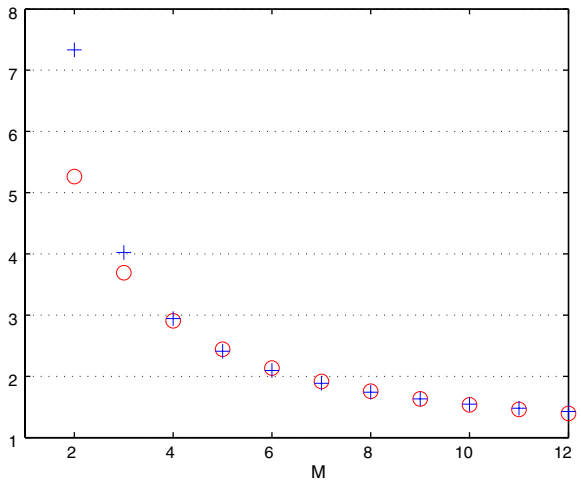

Fig. 8. Computational advantage factor: CH versus analog Monte Carlo, $g = 0.9$.

Next, in Fig. 7 we plot $\log_{10}$ of the mean square error for each method as a function of M. Note that with $M > 8$ and $N = 16$ the DSA error is $O(10^{-12})$ as we would expect, since with, say, 9 optical invariants preserved in the DSA model the corresponding radiance is, in fact, a P_{17} approximation, and should, therefore, agree with the analytically obtained P_{16} radiance. A similar argument applies in the $N = 20$ case. We observe that for $M \geqslant 3$ DSA is more accurate than ST, in conformity with the analysis presented in Section 7.

We supplement these estimates of accuracy with theoretical estimates of the computational advantage factor of the two CH methods when compared to analog Monte Carlo. This advantage is measured by the ratio of the scattering mean free paths: $\frac{1/\sigma_s^*}{1/\sigma_s}$. In Fig. 8, we plot these estimates as a function of M. We see that for small M, gains of at least a factor of 4 can be expected and that a factor of 2 or so should be expected when somewhat larger M values are chosen. Roughly speaking, then, the ST and DSA methods reduce the cost of analog Monte Carlo by a factor of 2 or more, with minimal effect on accuracy. This reinforces the data presented in Tables 2–4.

10. Conclusions

We have provided a brief review of condensed history methods, developed initially for modeling electron transport efficiently. Our treatment emphasizes the crucial role played by the Lewis–Larsen theory that relates low-order angular moments of the scattering phase function to low-order space-angle moments of the RTE solution. We have seen that the CCH model of Berger is substantially improved by both MCH and TCH methods that use the Lewis–Larsen theory, but problems remain, either (in the case of MCH) because of the increased costs when crossing interfaces and boundaries and those associated with sampling from density functions represented as infinite series, or because (in the case of TCH) the precision may be difficult to increase beyond $O(\lambda_s)$, where λ_s is the excess mean free path of the method.

These model shortcomings have led us to investigate two other CH methods that are also derivative of the Lewis–Larsen theory: similarity theory (ST) and the use of discrete scattering angles (DSA). In both of these cases, rather than determining the altered scattering properties from the desired increase in mean free path, the approximate scattering function is prescribed first through control of the number of angular moments to be preserved, and the resulting increase in mean free path is then uniquely specified from this constraint. Our analysis suggests that both of these methods should be useful in simulating photon transport in tissue. A feature of our implementation is that, by treating absorption of light continuously along the photon path, rather than as a discrete collision event, absorption can be treated consistently in both the exact and the approximate models and the relationship between altered scattering and increased mean free path is clarified. Since both of these methods model RTEs in a fully stochastic fashion, no special treatment of boundary and interface crossing is needed for them.

Both the theory and our numerical results seem to confirm that the discrete scattering angles CH method produces nearly twice the accuracy of similarity CH for comparable computational costs and that each is about twice as fast as analog Monte Carlo. Such gains are modest in comparison with the benefits reported for electron transport. We believe that the difference is due mainly to the more forward-peaked nature of electron scattering, as well as subtle, but important differences between the higher moments of the phase functions used for electron and photon scattering.

When the Henyey–Greenstein phase function describes the scattering of photons, the anisotropy factor, g, characterizes the phase function, and we observe that the predicted speed gains of CH MC over analog MC increase sharply as g approaches 1. To illustrate this point, we compare gains in speed for ST and DSA that preserve the same number, say 5, of optical invariants for two different values of g. For $g = 0.9$ and $g = 0.9999$ we compute gains for ST of 2.9 and 2500.4, while for DSA we obtain gains of 4.0 and 3273.4, respectively. This suggests that the use of alternative descriptions of photon scattering might prove to be useful experimentally and also enhance the advantages of using CH models in place of analog Monte Carlo.

In summary, we believe that the DSA method is the most promising for CH modeling of light-tissue interactions and deserves consideration when fast, but quite accurate, RTE solutions are needed. In future work, we plan to apply these CH modeling techniques to realistic, heterogeneous problems arising in biomedical optics.

Acknowledgments

This work was supported by the Laser Microbeam and Medical Program (NIH P41-RR-01192) at the Beckman Laser Institute, University of Irvine, California.

The authors would also like to acknowledge useful suggestions made by the referees.

Appendix A

In this appendix, we begin with the RTE

$$\frac{\partial \Phi(r,\omega;s)}{\partial s} + \omega \cdot \nabla \Phi + \sigma_t \Phi = \int_{4\pi} \sigma_s f(\omega' \cdot \omega) \Phi(r,\omega')\, d\omega' \tag{A.1}$$

of Section 3, subject to the identical assumptions, boundary conditions and notation adopted there. Our purpose here is to outline the derivation of the governing equation for the solution of (A.1) projected onto the depth axis, z.

We assume that scattering depends only on the scalar product of the unit vectors before and after collision, ω' and ω.[3] Then we can write

$$f(\omega' \cdot \omega) = \frac{1}{2\pi} f(\mu_0).$$

Now if we project the solution of (A.1) onto the depth axis, here denoted here by z, we obtain the function $\Phi = \Phi(z,\mu)$

$$\Phi(z,\mu) \equiv \int_0^{2\pi} \Phi(z,\omega') d\varphi = 2\pi \Phi(z,\omega').$$

In terms of the newly defined variables (A.1) becomes

$$\frac{\partial \Phi(z,\mu;s)}{\partial s} + \mu \frac{\partial \Phi}{\partial z} + \sigma_t \Phi = \frac{\sigma_s}{2\pi} \int_{4\pi} f(\mu_0) \Phi(z,\mu')\, d\omega'. \tag{A.2}$$

Next, we expand the phase function f in Legendre polynomials, P_n, in μ_0

$$f(\mu_0) = \frac{1}{2\pi} \sum_{n=0}^{\infty} \frac{2n+1}{2} f_n P_n(\mu_0), \tag{A.3}$$

where the expansion coefficients, f_n, are given by

$$f_n = \int_{-1}^{1} P_n(\mu_0) f(\mu_0)\, d\mu_0, \quad n = 0,1,2,\ldots$$

and we have made use of the orthogonality of the P_n. We note here that it can be shown that the Henyey–Greenstein phase function, f_{HG}, has the following property:

$$g^n = \int_{-1}^{1} P_n(\mu_0) f_{HG}(\mu_0)\, d\mu_0, \quad n = 0,1,2,\ldots$$

To proceed with the derivation we use the addition theorem for Legendre polynomials

$$P_n(\mu_0) = P_n(\mu) P_n(\mu') + 2 \sum_{m=1}^{n} \frac{(n-m)!}{(n+m)!} P_n^m(\mu) P_n^m(\mu') \cos[m(\varphi - \varphi')]. \tag{A.4}$$

Here $\mu = \cos(\theta)$ and the pair: (θ,φ) is, respectively, the polar and azimuthal angles that determine the direction ω. Now substitute (A.3) and (A.4) into (A.1). Then, since

[3] This follows from the rotational invariance of the scattering process.

$$\int_{4\pi}(*)\mathrm{d}\omega' = \int_0^{2\pi}\int_0^{\pi}(*)\sin\theta'\,\mathrm{d}\theta'\,\mathrm{d}\varphi' = \int_0^{2\pi}\int_{-1}^{1}(*)\,\mathrm{d}\mu'\,\mathrm{d}\varphi', \tag{A.5}$$

the integral in (A.2) becomes

$$\int_{4\pi} f(\mu_0)\Phi(z,\mu')\,\mathrm{d}\omega' = \int_0^{2\pi}\int_{-1}^{1}\sum_{n=0}^{\infty}\frac{2n+1}{2}f_n \cdot\left\{P_n(\mu)P_n(\mu') + 2\sum_{m=1}^{n}\frac{(n-m)!}{(n+m)!}P_n^m(\mu)P_n^m(\mu')\cos[m(\varphi-\varphi')]\right\}\Phi(z,\mu')\,\mathrm{d}\mu'\,\mathrm{d}\varphi'.$$

We next notice that if we integrate the last equation with respect to φ', the infinite series that contains the associated Legendre functions, P_n^m, vanishes because of the presence of the cosine term. Thus, we arrive at the following equation governing the (z,μ) problem:

$$\frac{\partial\Phi(z,\mu;s)}{\partial s} + \mu\frac{\partial\Phi(z,\mu;s)}{\partial z} + \sigma_{\mathrm{t}}\Phi(z,\mu;s) = \sigma_{\mathrm{s}}\int_{-1}^{1} f_{\mathrm{pl}}(\mu',\mu)\Phi(z,\mu';s)d\mu', \tag{A.6}$$

where

$$f_{\mathrm{pl}}(\mu',\mu) = \sum_{n=0}^{\infty}\frac{2n+1}{2}f_nP_n(\mu)P_n(\mu'). \tag{A.7}$$

Appendix B

In this Appendix we prove a theorem that validates the Lewis–Larsen theory of moments for planar geometry. We adopt the notation and assumptions of Appendix A and start with the transport equation for the (z,μ)-problem, Eq. (A.6). It can be shown [23,14] that the P_N equations corresponding to (A.6) are

$$\frac{\partial a_m(z;s)}{\partial s} + \frac{m+1}{2m+1}\frac{\partial a_{m+1}(z;s)}{\partial z} + \frac{m}{2m+1}\frac{\partial a_{m-1}(z;s)}{\partial z} + a_m(z;s)I_m = 0, \tag{B.1}$$

where $m = 0,1,2,\ldots$ Here a_m denotes the mth coefficient in the Legendre expansion of the radiance, Φ,

$$a_m(z;s) = \int_{-1}^{1}\Phi(z,\mu;s)P_m(\mu)\,\mathrm{d}\mu \tag{B.2}$$

and $I_m = \sigma_{\mathrm{t}} - \sigma_{\mathrm{s}}f_m$ denotes the mth optical invariant (Eq. (16)). We impose the following initial condition on Φ:

$$\Phi(z,\mu;0) = \delta(z)\delta(\mu-1). \tag{B.3}$$

Earlier we have defined the nth space and mth angular moment of Φ as $\Phi^{n,m}(s)$

$$\Phi^{n,m}(s) \equiv \int_{-\infty}^{\infty}\int_{-1}^{1} z^n\mu^m\Phi(z,\mu;s)\,\mathrm{d}\mu\,\mathrm{d}z. \tag{B.4}$$

Now we introduce the nth space and mth angular *Legendre* moment of Φ, $\Phi_L^{n,m}(s)$

$$\Phi_L^{n,m}(s) \equiv \int_{-\infty}^{\infty}\int_{-1}^{1} P_n(z)P_m(\mu)\Phi(z,\mu;s)\,\mathrm{d}\mu\,\mathrm{d}z = \int_{-\infty}^{\infty} a_m(z;s)P_n(z)\,\mathrm{d}z. \tag{B.5}$$

We observe that since any monomial of degree n can be expressed as a linear combination of Legendre polynomials up to the nth order, we can also express $\Phi^{n,m}$ as a linear combination of $\Phi_L^{n,m}$

$$\Phi^{n,m}(s) = \sum_{i=0}^{n}\sum_{j=0}^{m} c_{i,j}\Phi_L^{i,j}(s), \tag{B.6}$$

where $c_{i,j}$ are the coefficients of combination and $c_{n,m} \neq 0$. Next we derive a coupled system of ordinary differential equations for $\Phi_L^{n,m}$ which we state as

Lemma. *The functions $\Phi_L^{n,m}(s)$ satisfy the equations*

$$\frac{d\Phi_L^{0,m}(s)}{ds} + \Phi_L^{0,m}(s) I_m = 0, \quad n = 0, \ m = 0, 1, \ldots, \tag{B.7}$$

$$\frac{d\Phi_L^{n,m}(s)}{ds} - \sum_{i=0}^{[(n-1)/2]} \frac{2n-4i-1}{2m+1} \left[(m+1)\Phi_L^{n-2i-1,m+1}(s) + m\Phi_L^{n-2i-1,m-1}(s) \right] + \Phi_L^{n,m}(s) I_m = 0, \quad n > 0, \ m = 0, 1, \ldots \tag{B.8}$$

The initial condition here

$$\Phi_L^{n,m}(0) \equiv \int_{-\infty}^{\infty} \int_{-1}^{1} \delta(z)\delta(\mu - 1) P_n(z) P_m(\mu) \, d\mu \, dz = P_n(0) \tag{B.9}$$

follows from (B.3).

Proof. First, operate on Eq. (B.1) by $\int_{-\infty}^{\infty}(\cdot)P_0(z)\,dz$. The assumption that the radiance vanishes at infinity implies that the terms containing the derivatives with respect to z in (B.1) disappear. We obtain

$$\frac{d\Phi_L^{0,m}(s)}{ds} + \Phi_L^{0,m}(s) I_m = 0.$$

Next, operate on (B.1) by $\int_{-\infty}^{\infty}(\cdot)P_n(z)dz$, $n > 0$. This results in

$$\frac{d\Phi_L^{n,m}(s)}{ds} + \frac{m+1}{2m+1} \int_{-\infty}^{\infty} \frac{\partial a_{m+1}(z;s)}{\partial z} P_n(z)\,dz + \frac{m}{2m+1} \int_{-\infty}^{\infty} \frac{\partial a_{m-1}(z;s)}{\partial z} P_n(z)\,dz + \Phi_L^{n,m}(s) I_m = 0. \tag{B.10}$$

To simplify the integrals in (B.1) we use integration by parts

$$\int_{-\infty}^{\infty} \frac{\partial a_{m\pm1}(z;s)}{\partial z} P_n(z)\,dz = -\int_{-\infty}^{\infty} a_{m\pm1}(z;s) P_n'(z)\,dz. \tag{B.11}$$

Using (B.11) we can re-write (B.10) as

$$\frac{d\Phi_L^{n,m}(s)}{ds} + \frac{m+1}{2m+1} \int_{-\infty}^{\infty} a_{m+1}(z;s) P_n'(z)\,dz + \frac{m}{2m+1} \int_{-\infty}^{\infty} a_{m-1}(z;s) P_n'(z)\,dz + \Phi_L^{n,m}(s) I_m = 0 \tag{B.12}$$

Making use of elementary properties of Legendre polynomials [24] we can write P_n' as

$$P_n'(z) = (2n-1)P_{n-1}(z) + (2n-5)P_{n-3}(z) + (2n-9)P_{n-5}(z) + \cdots + \begin{cases} 3P_1(z), & \text{if } n \text{ is even} \\ P_0(z), & \text{if } n \text{ is odd} \end{cases}$$

$$= \sum_{i=0}^{[(n-1)/2]} (2n-4i-1) P_{n-2i-1}(z), \quad n = 1, 2, \ldots, \tag{B.13}$$

where square brackets in the upper limit of summation denote the integer part. Substituting the representation (B.13) of P_n' in (B.12), using the definition (B.5) of $\Phi_L^{n,m}$, we can re-write Eq. (B.10) in terms of $\Phi_L^{n,m}$. This results in (B.8) and completes the proof of the Lemma. □

Theorem. *The (n,m)th order spatial-angular moment of Φ, $\Phi^{n,m}(s)$, depends only on s and $I_k, k \leqslant n+m$.*

Proof. We prove the theorem by induction on n. First set $n = 0$ and write again Eq. (B.7) for $\Phi_L^{0,m}(s)$:

$$\frac{d\Phi_L^{0,m}(s)}{ds} + \Phi_L^{0,m}(s) I_m = 0$$

with the initial condition $\Phi_L^{0,m}(0) = 1$. The solution is, of course

$$\Phi_L^{0,m}(s) = e^{-I_m s}$$

and thus $\Phi_L^{0,m}$ depends on s and I_m for any m. Since Eq. (B.13) takes two forms depending on the parity of n, we also need to verify the theorem for $n = 1$ to begin the induction. That is, we want to show that $\Phi^{1,m}(s)$ depends only on s and I_k, $k \leqslant m + 1$. Putting $n = 1$ in (B.8) we get

$$\frac{\Phi_L^{1,m}(s)}{\mathrm{d}s} - \frac{m+1}{2m+1}\Phi_L^{0,m+1}(s) - \frac{m}{2m+1}\Phi_L^{0,m-1}(s) + \Phi_L^{1,m}(s)I_m = 0. \tag{B.14}$$

From the $n = 0$ case it follows that $\Phi_L^{0,m+1}$ depends on I_{m+1}, $\Phi_L^{0,m-1}$ depends on I_{m-1} and hence $\Phi_L^{1,m}$ depends on I_{m-1}, I_m, I_{m+1}. By (B.6) we can write

$$\Phi^{1,m}(s) = \sum_{j=0}^{m} c_{0,j}\Phi_L^{0,j}(s) + \sum_{j=0}^{m} c_{1,j}\Phi_L^{1,j}(s) \tag{B.15}$$

where $c_{0,m} \neq 0$, $c_{1,m} \neq 0$. The first term in (B.15) shows that $\Phi^{1,m}$ depends only on $I_0, \ldots, I_m$ while the second term brings in the dependence on I_{m+1} and thus the theorem is true for $n = 1$ and any m.

Suppose now that the theorem is true for some fixed n and arbitrary m; i.e. that $\Phi^{n,m}(s)$ is a function only of s and I_k, $k \leqslant n + m$. We want to show that $\Phi^{n+1,m}(s)$ is a function only of s and $I_k, k \leqslant n + m + 1$. Using (B.8) we write the equation for $\Phi_L^{n+1,m}$

$$\frac{\mathrm{d}\Phi_L^{n+1,m}(s)}{\mathrm{d}s} - \sum_{i=0}^{[n/2]} \frac{2n-4i+1}{2m+1}\left[(m+1)\Phi_L^{n-2i,m+1}(s) + m\Phi_L^{n-2i,m-1}(s)\right] + \Phi_L^{n+1,m}(s)I_m = 0 \tag{B.16}$$

Examining Eq. (B.16) reveals that $\Phi_L^{n+1,m}$ is defined in terms of $\Phi_L^{n-2i,m+1}$ and $\Phi_L^{n-2i,m-1}$ and thus the highest possible Legendre moment of the radiance determining $\Phi_L^{n+1,m}$ occurs for $i = 0$; i.e. it is $\Phi_L^{n,m+1}$. By the inductive assumption, $\Phi_L^{n,m+1}(s)$ depends on s and I_k, $k \leqslant n + m + 1$, establishing the theorem for $\Phi_L^{n+1,m}(s)$ and hence, by (B.6), for $\Phi^{n+1,m}(s)$ as well. □

References

[1] M.J. Berger, Monte Carlo calculation of the penetration and diffusion of fast charged particles, Nucl. Instrum. Methods Phys. Res. B 134 (1963) 135–215.
[2] S. Goudsmit, J.L. Saunderson, Multiple scattering of electrons, Phys. Rev. 57 (1940) 24–29.
[3] T.M. Jenkins, W.R. Nelson, A. Rindi, Monte Carlo Transport of Electrons and Photons, Plenum Press, New York and London, 1988.
[4] J.M. Fernandez-Varea, R. Mayol, J. Baro, F. Salvat, On the theory and simulation of multiple elastic scattering of electrons, Nucl. Instrum. Methods Phys. Res. B 73 (1993) 447–473.
[5] A.F. Bielajew, I. Kawrakow, On the condensed history technique for electron transport, Nucl. Instrum. Methods Phys. Res. B 142 (1998) 253–280.
[6] H.W. Lewis, Multiple scattering in infinite medium, Phys. Rev. 78 (5) (1950) 526–529.
[7] D.R. Tolar Jr., E.W. Larsen, The moment condensed history algorithm for Monte Carlo electron transport simulations, in: Proceedings of the ANS Topical Meeting: International Conference on Mathematical Methods to Nuclear Applications, Salt Lake City, Utah, September 9–13, American Nuclear Society, 2001.
[8] D.R. Tolar Jr., E.W. Larsen, A transport condensed history algorithm for Monte Carlo simulations, Nucl. Sci. Eng. 138 (1) (2001) 47–65.
[9] D.R. Wyman, M.S. Patterson, B.C. Wilson, Similarity relations for anisotropic scattering in Monte Carlo simulations of deeply penetrating neutral particles, J. Comput. Phys. 81 (1989) 137–150.
[10] A.K. Prinja, B.C. Franke, Monte Carlo electron dose calculations using discrete scattering angles and discrete energy losses, Nucl. Sci. Eng. 149 (1) (2005) 1–22.
[11] H. Neunschwander, T.R. Mackie, P.J. Reckwerdt, MMC – a high-performance Monte Carlo code for electron beam treatment planning, Phys. Med. Biol. 40 (1995) 543–574.
[12] I. Kawrakow, Accurate condensed history Monte Carlo simulation of electron transport EGSnrc, the new EGS4 version, Med. Phys. 27 (2000) 485–498.
[13] E.W. Larsen, Theoretical derivation of the condensed history algorithm, Ann. Nucl. Energy 19 (10-12) (1992) 701–714.
[14] G.I. Bell, S. Glasstone, Nuclear Reactor Theory, Van Nostran Reinhold, New York, 1970.
[15] D.R. Tolar, Advanced multiple scattering algorithms for electron transport, Ph.D. dissertation, University of Michigan, 1999.
[16] G.C. Pomraning, The Fokker–Planck operator as an asymptotic limit, Math. Models Methods Appl. Sci. 2 (1992) 21–36.
[17] C.L. Leakeas, E.W. Larsen, Generalized Fokker–Planck approximations of particle transport with highly forward-peaked scattering, Nucl. Sci. Eng. 137 (2001) 236–250.

[18] D.P. Sloan, A new multigroup Monte Carlo scattering algorithm suitable for neutral and charged particle Boltzmann and Fokker–Planck calculations, Ph.D. thesis, University of New Mexico, Albuquerque, NM, 1983.
[19] D.R. Wyman, M.S. Patterson, A discrete method for anisotropic angular sampling in Monte Carlo simulations, J. Comput. Phys. 76 (1988) 414–425.
[20] J. Spanier, E.M. Gelbard, Monte Carlo Principles and Neutron Transport Problems, Addison-Wesley Publishing Company, 1969.
[21] R.W. Hamming, Numerical Methods for Scientists and Engineers, Dover Publications, New York, 1973.
[22] E. Lewis, W.F. Miller Jr., Computational Methods of Neutron Transport, Wiley, New York, 1984.
[23] E.M. Gelbard, Spherical harmonics methods: P_L and double P_L approximations, in: H. Greenspan, C.N. Kelber, D. Okrent (Eds.), Computing Methods in Reactor Physics, Argonne National Laboratory, Gordon and Breach, 1969 (Chapter 4).
[24] J. Spanier, K.B. Oldham, An Atlas of Functions, Springer-Verlag, 1987.